Plasma-based X-ray laser speckle and its application on ferroelectric material

TAI Ren-Zhong[1], NAMIKAWA Kazumichi[2]

([1] Shanghai Institute of Applied Physics, the Chinese Academy of Sicences, Shanghai 201800, China; [2]Department of Physics, Tokyo Gakugei University, 4-1-1 Nukui-Kita Machi, Koganei-Shi, Tokyo 184-8501, Japan)

Abstract A new type of soft X-ray source, i.e. a plasma-based X-ray laser, is found to be promising to conduct transient measurement. By means of picosecond X-ray laser speckles, the dynamic microscopic polarization clusters within cubic (paraelectric) $BaTiO_3$ was directly observed and characterized in a microscopic scale for the first time. This opens a way to study this type of clusters, which usually manifest large external-field response for ferroelectric materials.

Key words Plasma-based X-ray laser speckle, Paraelectric $BaTiO_3$, Ferroelectric materials, Polarization cluster

CLC numbers O72, O738

1 Introduction

The development of coherent X-ray sources has made it possible to observe X-ray speckles.[1,2] X-ray speckles are produced by coherent X-ray scattering from disordered sample, where random constructive and destructive interferences by sample domains result in a speckle pattern. Speckle pattern depends on exact arrangement of domains, not just domain size distribution. If incident X-rays are not coherent, resolution is insufficient to observe speckle pattern. As Bragg diffraction peaks give detailed information for a crystal lattice, a speckle pattern contains important statistical information for the distribution of domains.

One important application of speckles is to measure time fluctuation. If domains fluctuate with time within a sample, then one can know the relaxation time of domains by measuring the time correlation of the speckles. This technique has been well applied for visible light since the invention of laser, but it is feasible only with the advent of modern X-ray sources, such as synchrotron radiation. A shorter wavelength can in general bring a higher resolution to domains; therefore it is the merit of X-ray speckles that they can be used to study fine structures which are usually invisible or inaccessible by means of visible laser.

So far, by means of synchrotron radiation X-ray sources, X-ray speckles have been applied to many objects, for example, gold/Pd/Sb_2O_5/latex colloids, PS-PI block copolymer micelles in PS, hexane/nitrobenzene binary fluids, anti-phase domains in metal alloys, phase separation in sodium borosilicate glasses, and PS/PB homopolymer mixtures, etc.[3-6]

Plasma-based soft X-ray laser is another kind of powerful X-ray source,[7-9] although it has been rarely used due to its single-shot feature. Nevertheless, the quality of this X-ray source is almost comparable to future X-ray free electron laser (XFEL).[10] X-ray lasers operated in a transient collisional excitation scheme have very short pulse duration (about 7 ps), within which about 10^{12} photons assemble.[9] One pulse of X-ray laser can provide sufficient detectable X-ray photons, the transient X-ray measurement hence becomes feasible. From the viewpoint of methodology, present X-ray lasers provide appropriate sources to study some prototype experiments for future XFEL, even if its photon energy is single and untunable.

We chose $BaTiO_3$ as the sample because there are a lot of controversies on the basic problem such as the mechanism of phase transition, though it has been applied extensively and studied intensively.[11] The

Received date: 2005-04-29

paraelectric-ferroelectric phase transition for this prototype ferroelectric substance has long been thought as a classic displacive soft-mode type,[12,13] whereas anomalies were also known near the phase transition temperature, which was unable to be interpreted simply by a displacive type.[14,15] As measured by Hyper-Raman spectroscopy,[16,17] a relaxational dynamics was also observed in the paraelectric $BaTiO_3$ near T_c. NMR experiment[18] has recently shown that Ti ion in the paraelectric phase of $BaTiO_3$ flutters among off-center sites, claiming the coexistence of order-disorder and displacive characters in phase transition of $BaTiO_3$ as that predicted by simulation.[19] However, it is not clear how a stable ferroelectric polarization domain turns up from those paraelectric fluctuating dipole moments, in particular, how the dipoles fluctuations correlate spatially each other and evolve into a ferroelectric domain as T_C is approaching. Experimental clarification of the dynamic dipole clusters within $BaTiO_3$ is one of the most important issues in the field of ferroelectrics.

Molecular dynamic simulations[19] and theory,[20] concerning the phase transition mechanism, have shown existence of polarization clusters in paraelectric $BaTiO_3$ near T_C. Although experiments such as neutron scattering,[21] X-ray scattering,[15,22] and optical birefringence[23,24] showed strong fluctuating polarizations existing in paraelectric phase of $BaTiO_3$ near T_C, such clusters have never been directly observed to date. The reason lies in the fact that the relaxation time of a particular cluster, around an order of nanoseconds,[16,18] is too short compared to the general measuring time in practice. Traditional diffuse X-ray scattering or neutron scattering cannot be used to observe the dynamic correlation length, because where the spatial correlation has been averaged by the much longer measuring time. X-ray speckles by synchrotron radiation are also difficult to resolve such a nanosecond order even when we use time correlation technique. The inherent noise correlation from electron bunches prevent us from recognizing useful signal with a time order less than microseconds. Therefore, picosecond transient measurement of the speckles by means of X-ray laser seems to be a unique way at present to observe the behavior of those dynamic clusters.

So far, several experiments by means of picosecond X-ray laser speckles on $BaTiO_3$ have been conducted at the Advanced Photon Research Center, Japan Atomic Energy Research Institute. The main results have been reported elsewhere.[25-27] In this text, we will give a detailed description of the experiment, placing emphasis on the analysing method. Lastly, we will give a prospect of this method for other materials.

2 Experimental setup

The experimental setup is schematically shown in Fig.1. The X-ray laser media here is a silver plasma produced by a chirped-pulse-amplification Nd:glass pump laser light focusing on a silver target.[9] The lasing line is the transition of $3d^94d \rightarrow 3d^94p$, with a wavelength of 13.9 nm and a bandwidth of $\Delta\lambda/\lambda \sim 10^{-4}$. The X-ray laser pulse duration is estimated to be 7 ps. The X-ray laser beam has been characterized to have a source size of 50μm and a divergence angle of 10 mrad.[28] The total photons are about 10^{12} per pulse.

A 45° incidence Mo/Si multilayer was used to produce a vertically polarized X-ray probing beam. A small aperture located at 1.9 m (about 0.5 m from Mo/Si mirror) from the plasma source was used to produce a fully coherent X-ray photon beam. The sample used in experiment was a flux-grown ferroelectrics $BaTiO_3$ single crystal with alternative *a/c* domains aligned in parallel at room temperature. The Curie temperature T_C was 122℃. The sample was set to locate close to the slit, with its domain boundaries (walls) directed along the vertical direction. The temperature of the sample was controlled with a precision of ±0.1℃. A high DC voltage slab electrode was set at the 2.5 mm front of the specimen, which can produce a uniform high electric field (2 kV/cm was selected for the data shown) normal to the specimen surface. The local electric field E_x within the specimen was estimated to be 0.4 V/cm, if we suppose the static dielectric constant ε_x to be 5000 at 123.5℃. This value is near to that commonly used to measure the ε_x near T_C, and hence believed to be sufficiently large to reverse the clusters' polarizations. The grazing angle was 10°. The diffracted speckle patterns were recorded by a soft X-ray charge-coupled device (CCD).

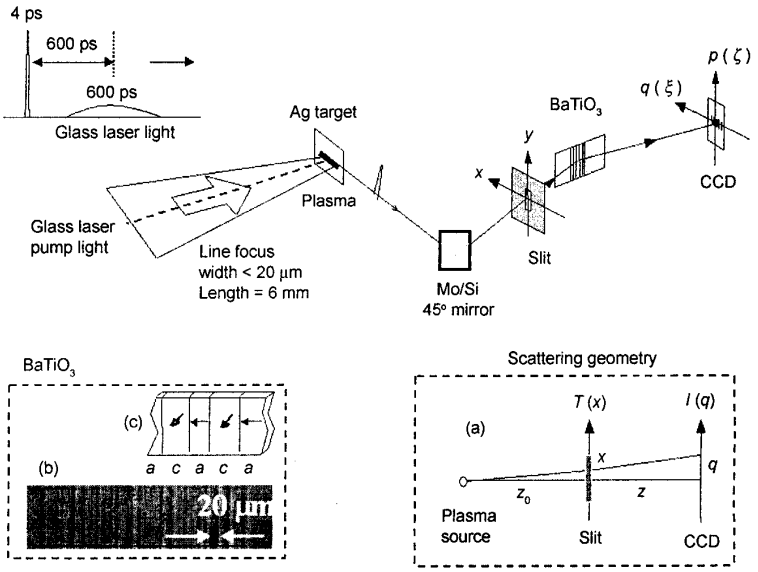

Fig.1 Experimental setup.

3 Results

Fig.2 shows those patterns below T_C, where the aperture was set to be 80 μm (horizontal) ×200 μm (vertical) and the CCD was set to be 0.5 m far from the sample. The transverse (horizontal) resolution of this setup is estimated to be around 1 μm. For comparison the probing beam pattern is given in Fig.2(a). Fig. 2(b)-2(h) show a series of the speckles diffracted from a region of multiple *a*/*c* domains when heating the sample from 24℃ to 130℃. These two obvious groups in Fig.2(b) and 2(c) indicate that, at lower temperatures, *a* domains and *c* domains constitute respectively two groups of planes with a normal angle determined by the temperature-dependent *a*/*c* twin angle.[29] The speckles in each of the two groups originated from the interference of X-ray photons scattered by the same type of domains (for instance, *a* domains), where the other type of domains (*c* domains) were invisible. This has been schematically shown on the right bottom of Fig.2. As temperature increased toward the Curie temperature T_C, the pattern apparently evolved into one group, indicating the adjacent *a*/*c* twin angles are getting smaller and more irregular even at the same temperature. Above T_C, the speckles turned into one spot, as shown in Fig.2(h), indicating the disappearance of the domains.

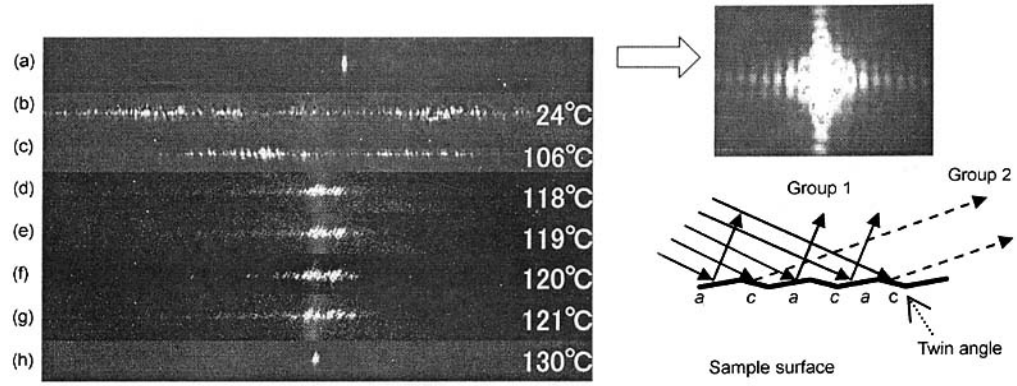

Fig.2 Speckle patterns diffracted from alternative *a*/*c* 90° domains.

Above T_C, we still found that there are some small structures near the main peak. To study this phenomenon carefully, the setup has been little modified to enhance the performance. The distance of CCD was reduced to 0.2 m. The aperture was set to be 200 μm (horizontal) ×80 μm (vertical). Then the vertical spatial resolution on the sample was estimated to be 0.2 μm. We focussed on the study of the vertical tail structure of the patterns. The results show that this kind of tail depends strongly on temperature and the external DC electric field E. As shown in Fig.3, the tail increased as temperature was lowered toward T_C, and decreased dramatically if E was applied, which indicates that the scatterers within the sample are dipole-related and temperature-dependent. Those scatterers are in fact the polarization clusters.

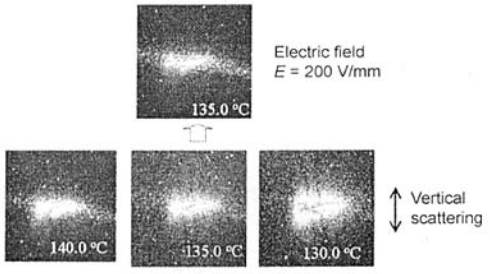

Fig.3 Speckle patterns from clusters above T_c.

4 Birefringence model

The coherent scattering mechanism is shown in Fig.4 from the view of polarization clusters. Experiments have shown evidence that the clusters polarize preferably along the crystallographic axis (x; y, or z in Fig.4).[13,21] By a picosecond y-polarized X-ray illumination, these clusters with polarizations along the y or -y are spatially recorded on the phase of the scattered beam due to the birefringence. The x- or z-polarized clusters would be indistinguishable from the noncluster region (cubic), since they all exhibit an ordinary refraction index for the grazing incident X-ray beam. The additional phase from the ith y-polarized cluster is estimated to be $\Delta\phi_i$:

$$\Delta\phi_i = 2\pi l \mathrm{Re}(\varepsilon_{33}^{1/2} - \varepsilon_{11}^{1/2})_i / \lambda \qquad (1)$$

where l is the average X-ray path length within the specimen, ε_{ii} is the dielectric tensor. The experiment was carried out with a 89 eV coherent photon beam and the scattering angle off the sample surface was 10°. This angle, being less than the critical angle (14°), implies that our experiment is sensitive to correlations at surface of the sample alone. The photon energy is 89 eV, near the binding energy of the $N_5 4d_{5/2}$ electrons in Ba.[30] Therefore, it can be anticipated that the anomalous dispersion would contribute a nontrivial value to the $\Delta\phi_i$. The X-rays due to spatial phase modulation interfere each other to give rise to the speckle patterns.

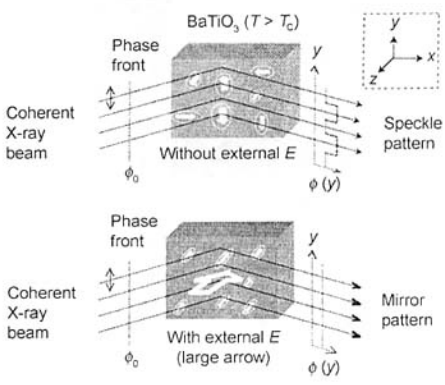

Fig.4 Schematic diagram of the coherent scattering mechanism of polarization clusters due to birefringence.

5 Dynamic features

One interesting feature of the tail structures is their shot-by-shot fluctuations. As shown in Fig.5(a), a strong shot-by-shot fluctuation was found at the same temperature (shown is 123.5 ± 0.1℃) in the vertical speckle profile. This fluctuation was clearly much larger than the accidental noise of CCD count denoted as the error bar in the figure. For comparison, the single-shot profile with an external DC high electric field E applied normally to the surface was also shown in the figure. Therefore, the shot-by-shot fluctuations in the speckle profile arise from dynamic nature of those scatterers.

A statistical average over ten shots at 123.5℃ is shown in Fig.5(b). For comparison, the single-shot profile at 123.5℃ with a high E applied and the single-shot profile at 140.0℃ are also shown. The good coincidence of these two profiles indicates that they are approaching to the specular reflection from the corrugated surface. The multi-shots average is equivalent to the statistical average of those scattering structures within the sample. The small discrepancy at

the tail and at the peak arises from the finite statistical number (ten shots). The coincidence of the ten-shots-averaged profile to the other two ones, combined with the feature of shot-by-shot fluctuations as shown in Fig.5(a), clearly indicates that those scatterers observed from speckles are indeed both dynamically and spatially randomly distributed.

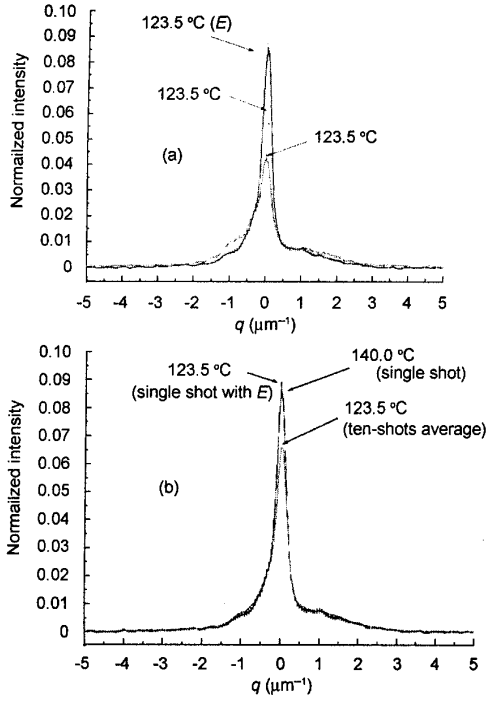

Fig.5 Cross-sectional vertical intensity distributions shot by shot above T_C.

The coincidence of these three profiles in Fig.5(b) also indicates another fact that those static surface structures (such as surface corrugation) have no significant change within the observed temperatures. Since we have used the profile at 140.0℃ as the specular pattern in extracting the matter correlation function as described in the following part, the undesirable effects such as the static surface corrugation are compensated to a negligible level.

6 Analyses

Speckle patterns contain detailed statistic distribution information of those scatterers within the studied sample. In practice, the illuminating beam is usually spatially confined in order to obtain a fully coherent beam, which inevitably results in a special spatial distribution for the probing beam. The speckle patterns are in fact a result of the convolution of diffraction of the confined beam with that of microscopic scatterers. Now we will show how to extract the useful information related only with scatterers.

Now suppose we study only the distribution along x-direction, i.e. horizontal direction. Of course this method is also applicable to y-direction distribution. We can generally use a complex transmittance $T(x) = T_0(x) \exp[i\phi(x)]$ to describe domains or clusters projected on the slit, where the real part $T_0(x)$ stands for the X-ray amplitude transmittance and the $\phi(x)$ for the X-ray phase retardation respectively from the specimen. The x is the horizontal coordinate along the x-axis as shown in Fig.1. The $T_0(x)$ is of course zero if the x falls beyond the slit, that is $|x| > D/2$, where D is the horizontal width of the slit. The complex transmittance $T(x)$ carries the information of the spatial distribution of those scatterers. The matter correlation function may be defined as

$$\gamma(\Delta x) = \frac{\int_{-\infty}^{\infty} T(x')T^*(x'+\Delta x)\,\mathrm{d}x'}{\int_{-\infty}^{\infty} T(x')T^*(x')\,\mathrm{d}x'} \qquad (2)$$

From a point-source approximation, as shown in the inset (a) of Fig.1, the intensity scattered into a direction of $(\boldsymbol{k}+\boldsymbol{q})$ can be written as follows according to the Fresnel-Kirchhoff diffraction integral[31]

$$I(q) = \int_{-\infty}^{\infty}\int_{-\infty}^{\infty} \mathrm{d}x\,\mathrm{d}x' T(x)T^*(x') \times \exp\left[ik\left(\frac{1}{2z_0}+\frac{1}{2z}\right)(x^2-x'^2) - iq(x-x')\right] \qquad (3)$$

where z_0, z are the distance of the slit from the source and the CCD respectively, $\boldsymbol{k}$ is the wave vector of incident X-ray photons, and $\boldsymbol{q}$ is the scattering vector defined as $\boldsymbol{q}=k\xi/z\boldsymbol{e}_\xi$, where ξ is the coordinate on CCD along the diffraction direction with a unit vector $\boldsymbol{e}_\xi$. The high-order terms of x have been omitted due to their negligible contribution to the integration, considering z_0, $z >> D$ in practice. The diffraction pattern is a convolution of the slit diffraction and the domains structure diffraction.

Considering the randomness of domain size or cluster size, the Fourier transform of Eq. (2) can be factorized simply as

$$\Gamma(x) = \mathrm{F}\{I(q)\} = \gamma(\Delta x) \times \Gamma_0(\Delta x) \quad (4)$$

where $\Gamma_0(\Delta x)$, defined as follows, is the apparatus function:

$$\Gamma_0(x) = \int_{-D/2}^{D/2-x} \exp[ik(\frac{1}{2z_0}+\frac{1}{2z})x'^2 - ik(\frac{1}{2z_0}+\frac{1}{2z})(x+x')^2]dx' \quad (5)$$

As shown in Eq.(5), the $\Gamma_0(x)$ is determined only by the geometric parameters of experimental setup, such as the slit width, the distances from the source and the CCD, and more, the properties of the source. It can be obtained from the Fourier transform of the specular reflection $I_{Sp}(q)$ in practice. The matter correlation function can be further expressed in a compact form as

$$\gamma(\Delta x) = \frac{\mathrm{F}[I(q)]}{\mathrm{F}[I_{Sp}(q)]} \quad (6)$$

from an experimental viewpoint, where F denotes the operation of Fourier transformation.

Since we feel interested in the phase modulation by clusters, now we show how to obtain cluster information from matter correlation function. We turn to y-direction distribution of clusters as shown in Fig.4. In this case, the matter correlation function as defined in Eq.(2) is simplified as

$$\gamma(\Delta y) = \frac{1}{D_y}\left\langle \exp\{i[\phi(y+\Delta y)-\phi(y)]\}\right\rangle_y \quad (7)$$

where the angular bracket denotes an ensemble average along y; $\phi(y)$ is the phase distribution instantaneously viewed by single-shot X-ray beam; D_y is the slit width in the vertical direction.

The parameters extracted from $\gamma(\Delta y)$ as follows are pure simplified one-dimensional parameters of the clusters (y-directional distribution). The mean size σ_s of clusters can be naturally considered to be the half width of the autocorrelation part of $\gamma(\Delta y)$. If we denote the mean distance of the clusters as d, then $\gamma(d/2)$ must be the first minimum from the origin of the profile of $\gamma(\Delta y)$. The correlation depth is defined as

$$\Delta\gamma_m = \gamma(0) - \gamma(\frac{d}{2}) \quad (8)$$

where the $\gamma(0)$ is 1, indicating the maximum autocorrelation. Suppose the additional phase given by the ith cluster to be

$$\Delta\phi_i = \frac{2\pi l}{\lambda}\Delta n_i \quad (9)$$

where l is X-ray path length within sample and the Δn_i is additional refraction index due to cluster compared to the cubic matrix. The correlation depth can be expressed as

$$\Delta\gamma_m = \frac{\sigma_S}{4d}\left(\frac{\lambda}{l}\right)^2\left\langle(\Delta n)^2\right\rangle \quad (10)$$

The random distribution of the polarization magnitudes in the clusters suggests:

$$\left\langle(\Delta n)^2\right\rangle = 2\left\langle\Delta n\right\rangle^2 \quad (11)$$

from a statistic viewpoint. The polarization in the cluster relates the refractive index difference by the quadratic Kerr effect, so we can estimate the mean polarization magnitude within the clusters as

$$|P| \propto \left\langle\Delta n\right\rangle^{1/2} \quad (12)$$

Substituting Eq.(11) and Eq.(12) for Eq.(10), we got

$$|P| \propto \left(\frac{l}{\lambda}\right)^{1/2}\left(\Delta\gamma_m\frac{d}{\sigma_S}\right)^{1/4} \quad (13)$$

Since correlation depth $\Delta\gamma_m$, cluster's size σ_S, and clsuters' distance d can be directly measured from the matter correlation function as described above, we can easily estimate the polarization within the clusters according to Eq.(13).

7 Discussion

Fig.6 shows the extracted physical parameters of the clusters according to the analyzing method described above. Fig.6(a) shows the evolutions of the mean size σ_s and the mean distance d of those y-polarized clusters with respect to the temperature. There seems no significant change of the cluster size observed in the experiment. However, the distance increases with temperature approximately linearly with a fitting slope of 0.33μm/℃. By extrapolating the two dashed lines (linear fitting) in Fig.6(a), one may find a crossover at a lower temperature T_D (estimated

to be 6℃ below T_C, not drawn in the figure). The T_D might be understood as a temperature where dynamic clusters have completely condensated into a ferroelectric domain. Fig.6(b) shows the mean magnitude $|P|^2$ of the polarizations within clusters, where a peak was observed at temperature about 5℃ above T_C. Molecular dynamic simulations[19] have shown that a crossover from displacive to order-disorder transition exists in the vicinity of T_C. The temperature for this crossover might be estimated from that of the peak of the $|P|^2$. As shown in the figure, as temperature approaches T_C, the $|P|^2$ behaves monotonically increasing at relatively higher temperatures, indicating the increase of the cooperative motions among Ti ions within the cluster. However, this increase was observed to stop at a temperature very close to T_C, implying the breaking of the cooperative motions of particles near phase transition due to the increase of fluctuation of dipole moment among off-center sites.

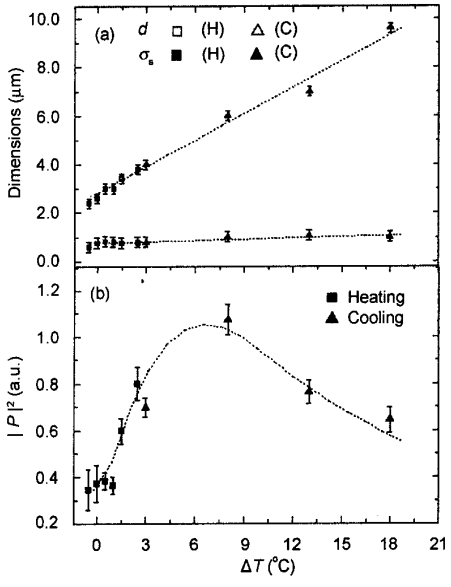

Fig.6 The temperature evolution of the characteristic parameters of clusters.

The macroscopically averaged polarization within the specimen may be defined as $(\sigma_s/d)^3|P|$ from a three dimensional viewpoint. We show the temperature dependence of this physical quantity in Fig.7. The quasi-linear behavior at higher temperatures in Fig.7 is completely consistent with that measured by Burns[23] and Takagi[24] with the use of birefringence of visible laser. Nevertheless, the picosecond X-ray speckle's measurement provides a new feature as shown in the lower temperature region near T_C in Fig.7. The macroscopically averaged polarization diverges as temperature approaches T_C. We can give an alternative expression for this quantity as $G=(1/d)^3(\sigma_s^3|P|)$, which is in fact the dipole potential that the adjacent clusters feel each other, and hereafter called the short-range correlation strength of the local clusters. From the inset of Fig.7, one can clearly see that the clusters' short-range correlation strength G increases in a form of power law $\mu^{-\kappa}$ as temperature approaches T_C, where μ is the reduced temperature defined as $\mu=(T-T_C)/T_C$. The critical exponent κ is determined to be 0.41±0.02 by a least square fitting.

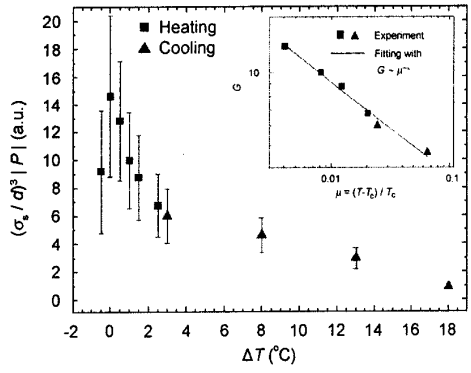

Fig.7 The temperature evolution of the macroscopically averaged polarization fluctuations within the paraelectric (cubic) $BaTiO_3$.

8 Conclusion

A speckle method has been established by means of single-shot plasma-based soft X-ray laser. With this technique, the dynamic polarization clusters in the paraelectric $BaTiO_3$ near T_C have been observed at surface for the first time. This dynamic polarization cluster provides a direct information of the spatial correlation of those fluctuating dipole moments in surface during phase transition. The knowledge of such spatial correlation of fluctuating dipole moments plays also an essential role in understanding the nature of the relaxor ferroelectrics[32] or the quantum paraelectrics.[33]

The relaxation time of the clusters would be another important parameter. This might be observed from time correlation of two photons scattered at a certain q position of the speckles.

Acknowledgements

Tai Renzhong would like to express his great thanks to the kind cooperation of X-ray laser group, Advanced Photon Research Center, JAERI. He will also thank Prof. Akikatsu Sawada (Okayama U.) for kind provision of the sample and for the much stimulating discussions. His thanks will also extend to Prof. Masami Ando (KEK, PF), Prof. Peixiang LU (Huazhong U. of Sci. and Tech.), Prof. Hiroshi Maruyama (Hiroshima U.) for valuable advices for this study.

References

1 Sutton M, Mochrie S G J, Greytak T, *et al.* Nature, 1991, **352**: 608

2 Cai Z H, Lai B, Yun W B, *et al.* Phys Rev Lett, 1994, **73**: 82

3 Brauer S, Stephanson G B, Satton M, *et al.* Phys Rev Lett, 1995, **74**: 2010

4 Lurio L B, Lumma D, Sandy A R, *et al.* Phys Rev Lett, 2000, **84**: 785

5 Yakhon F, Letoublon A, Livet F, *et al.* ESRF Newsletter, 1999, **32**: 12

6 Mochrie S G, Mayers A M, Sandy A R, *et al.* Phys Rev Lett, 1997, **78**: 1275

7 Key M H. Nature (London), 1985, **316**: 314

8 Daido H. C R Acad Sci Paris, 2000, **4**: 999

9 Kawachi T, Tanaka M, Hasegawa N, *et al.* Phys Rev, 2002, **A 66**: 033815

10 See, for example, DESY Report No. 2001-011, edited by Materilik G and Tschentscher Th, 2001

11 See, for example, Xu Y, Ferroelectric material and their applications, Amsterdam: Elsevier Science, 1991

12 Cochran W. Adv Phys, 1960, **9**: 387; 1961, **10**: 401

13 Harada J, Axe J D, Shirane G. Phys Rev, 1971, **B 4**: 155

14 Luspin Y, Servoin J L, Gervais F. J Phys, 1980, **C 13**: 3761

15 Comes R, Lambert M, Guinier A. Solid State Commun, 1968, **6**: 715

16 Vogt H, Sanjurjo J A, Rossbroich G. Phys Rev, 1982, **B 26**: 5904

17 Inoue K. Ferroelectrics, 1983, **52**: 253

18 Zalar B, Laguta V V, Blinc R. Phys Rev Lett, 2003, **90**: 037601

19 Stachiotti M, Dobry A, Migoni R, *et al.* Phys Rev, 1993, B **47**: 2473

20 Takahasi H. J Phys Soc Jpn, 1961, **16**: 1685

21 Yamada Y, Shirane G, Linz A. Phys Rev, 1969, **177**: 848

22 Motegi H, Mitsui T. J Phys Chem Solids, 1964, **25**: 253

23 Burns G, Dacol F H. Solid State Commun, 1982, **42**: 9

24 Takagi M, Ishidate T. Solid State Commun, 2000, **113**: 423

25 Tai R Z, Namikawa K, Kishimoto M, *et al.* Phys Rev Lett, 2002, **89**: 257602

26 Tai R Z, Namikawa K, Sawada A, *et al.* Phys Rev Lett, 2004, **93**: 087601

27 Tai R Z, Namikawa K, Kishimoto M, *et al.* in Eighth International Conference on Synchrotron Radiation Instrumentation, San Francisco, California, 2003, edited by Warwick T *et al.*, AIP Conf. Proc. No. 705 AIP, New York, 2004: 1122

28 Tang H, Daido H, Kishimoto M, *et al.* Jpn J Appl Phys Part 1, 2003, **42**(2A): 443

29 Takashige M, Hamazaki S, Takahashi Y, *et al.* Jpn J Appl Phys, Part 1, 1999, **38**: 5686

30 Thompson A C, Lindau I, Attwood A, *et al.* X-ray data booklet, Berkeley, California, 2001: 1-5

31 Born M, Wolf E. Principles of optics, Oxford: Pergamon, 1965: 382, 680

32 Gehring P M, Wakimoto S, Ye Z G, *et al.* Phys Rev Lett, 2001, **87**: 277601

33 Ang C, Yu Z, Jing Z. Phys Rev, 2000, **B 61**: 957